

# Orbitally Forced Ice Sheet Fluctuations in Snowball Earth

Douglas I. Benn,<sup>1,2\*</sup> Guillaume Le Hir,<sup>3</sup> Huiming Bao,<sup>4</sup> Yannick Donnadieu,<sup>5</sup> Christophe Dumas,<sup>5</sup> Edward J. Fleming,<sup>1,6,7</sup> Michael J. Hambrey,<sup>8</sup> Emily A. McMillan,<sup>6</sup> Michael S. Petronis,<sup>9</sup> Gilles Ramstein,<sup>5</sup> Carl T.E. Stevenson,<sup>6</sup> Peter M. Wynn,<sup>10</sup> Ian J. Fairchild<sup>6</sup>

---

<sup>1</sup>Department of Geology, The University Centre in Svalbard (UNIS), N-9171 Longyearbyen, Norway.

<sup>2</sup>School of Geography and Geosciences, University of St Andrews, St Andrews KY16 8YA, Scotland, UK.

<sup>3</sup>Institut de Physique du Globe de Paris, Paris, France

<sup>4</sup>Department of Geology and Geophysics, E235 Howe-Russell Complex, Louisiana State University, Baton Rouge, LA 70803, USA.

<sup>5</sup>Laboratoire des Sciences du Climat et de l'Environnement, CNRS-CEA, Gif-sur-Yvette, France

<sup>6</sup>School of Geography, Earth and Environmental Sciences, University of Birmingham B15 2TT, UK.

<sup>7</sup>Current address: CASP, West Building, 181A Huntingdon Road, Cambridge, CB3 0DH, UK

<sup>8</sup>Institute of Geography and Earth Sciences, Aberystwyth University, Aberystwyth, Wales, UK.

<sup>9</sup> Natural Resource Management, Environmental Geology,, New Mexico Highlands University, Las Vegas, New Mexico, USA.

<sup>10</sup>Lancaster Environment Centre, University of Lancaster, Lancaster LA1 4YQ, UK.

\*Corresponding author. E-mail: [Doug.Benn@unis.no](mailto:Doug.Benn@unis.no)

1 Snowball Earth theory provides a powerful framework for understanding  
2 Neoproterozoic panglaciations, although some predictions are apparently  
3 contradicted by geological evidence. Snowball theory posits that the  
4 panglaciations were terminated after millions of years of fridity by a positive  
5 feedback, in which initial warming from rising atmospheric CO<sub>2</sub> was amplified by  
6 reduction of ice cover and planetary albedo (1, 2). This threshold behaviour implies  
7 that most of the glacial record was deposited in a brief 'melt-back' period (3), an  
8 interpretation apparently inconsistent with geological evidence for glacial-  
9 interglacial cycles in low palaeolatitudes (4-6). Here we use geological and  
10 geochemical evidence combined with numerical modeling experiments to  
11 reconcile these apparently conflicting views. New evidence from Svalbard  
12 (Norwegian High Arctic) indicates oscillating glacier extent and hydrological  
13 conditions within continental deposits of a Cryogenian glaciation, during a period  
14 when  $p\text{CO}_2$  was uniformly high. Modeling experiments show that such oscillations  
15 can be explained by orbital forcing in the late stages of a 'Snowball' glaciation,  
16 while  $p\text{CO}_2$  was rising towards the threshold required for complete melt-back. This  
17 enriched Snowball Earth theory can potentially explain complex successions  
18 observed at other localities.

19 The Wilsonbreen Formation in NE Svalbard contains a detailed record of  
20 environmental change during the Marinoan, the second of the major Cryogenian  
21 glaciations (650-635 Ma) (7, 8). At this time, Svalbard was located in the Tropics on  
22 the eastern side of Rodinia (9, 10). The <180 m thick Wilsonbreen Formation was  
23 deposited within a long-lived intracratonic sedimentary basin (11). It is subdivided  
24 into three members (W1, W2 and W3) based on the relative abundance of diamictite

25 and carbonate beds (7, 8; Fig. 1; Supplementary Figures 1 & 2). The occurrence  
26 throughout the succession of lacustrine sediments containing both precipitated  
27 carbonate and ice-rafted detritus, and intermittent evaporative carbonates and  
28 fluvial deposits, indicates that the basin remained isolated from the sea, consistent  
29 with eustatic sea level fall of several hundred metres and limited local isostatic  
30 depression (Supplementary Information; 12). This makes it ideal for investigating  
31 environmental change within a Neoproterozoic panglaciation, as it provides direct  
32 evidence of subaerial environments and climatic conditions.

33 We made detailed sedimentary logs at ten known and new localities extending  
34 over 60 km of strike (Fig. 1; Supplementary Figure 1; see Methods). Seven sediment  
35 facies associations were identified, recording distinct depositional environments that  
36 varied in spatial extent through time (Supplementary Figure 3; Supplementary  
37 Information). These are: FA1: *Subglacial*, recording direct presence of glacier ice,  
38 FA2: *Fluvial channels*, FA3: *Dolomitic floodplain*, recording episodic flooding,  
39 evaporation and microbial communities; FA4: *Carbonate lake margin*, including  
40 evidence of wave action; FA5: *Carbonate lacustrine*, including annual rhythmites and  
41 intermittent ice-rafted debris; FA6: *Glacilacustrine*, consisting of ice-proximal  
42 grounding-line fans (FA6-G) and ice-distal rainout deposits (FA6-D); and FA7:  
43 *Periglacial*, recording cold, non-glacial conditions. Additional descriptions are  
44 provided in the Supplementary Information. The vertical and horizontal distribution  
45 of these facies associations (Fig. 1) allows the sequence of environmental changes to  
46 be reconstructed in detail.

47 (1) The base of the Formation is a well-marked periglacially weathered horizon  
48 with thin wind-blown sands (Supplementary Figure 4a-b). This surface records very  
49 limited sediment cycling in cold, arid conditions.

50 (2) At all localities, the weathering horizon is overlain by fluvial channel facies  
51 (FA2) and mudstones, marking the appearance of flowing water in the basin and  
52 implying positive air temperatures for at least part of the time (Supplementary  
53 Figure 5a).

54 (3) Glacilacustrine deposits (FA6-D) record flooding of the basin and delivery of  
55 sediment by ice-rafting (Supplementary Figure 4c-d). Far-travelled clasts are  
56 common, indicating transport by a large, continental ice sheet.

57 (4) Warm-based, active ice advanced into the basin, indicated by traction tills and  
58 glacitectonic shearing (FA1; Supplementary Figure 4e-g). (1 – 4 make up Member  
59 W1.)

60 (5) Ice retreat is recorded by a second periglacial weathering surface (FA7). This is  
61 overlain by fluvial channel, floodplain, lake-margin and carbonate lacustrine  
62 sediments of W2 (FA2-5; Supplementary Figure 5), recording a shifting mosaic of  
63 playa lakes and ephemeral streams. Lakes and river channels supported microbial  
64 communities. Millimetre-scale carbonate-siliciclastic rhythmites indicate seasonal  
65 cycles of photosynthesis. The environment appears to have been closely similar to  
66 that of the present-day McMurdo Dry Valleys in Antarctica, though with less extreme  
67 seasonality due to its low latitude (13).

68 (6) Water levels and glacier extent underwent a series of oscillations, recorded by  
69 switches between glacilacustrine diamictite (FA6-D) and fluvial, lacustrine and lake-

70 margin sediments (FA2-5) in W2. Sedimentation rates inferred from annual  
71 rhythmites in W2 suggest that each retreat phase may have lasted  $\sim 10^4$  years.

72 (7) A second major ice advance marks the base of W3, with widespread  
73 deposition of subglacial tills and glacitectonism of underlying sediments. Basal tills  
74 are absent from the northernmost locality, but close proximity of glacier ice is  
75 recorded by grounding-line fans (FA6-G; Supplementary Figure 4h-i).

76 (8) Ice retreated while the basin remained flooded and glacial sediment  
77 continued to be delivered to the lake by ice rafting. Thin laminated carbonates (FA5)  
78 in W3 indicate periods of reduced glacial sedimentation, indicative of minor  
79 climatic fluctuations over timescales of  $\sim 10^3$  years (Supplementary Figure 5g).

80 (9) A sharp contact with overlying laminated 'cap' carbonate (Supplementary  
81 Figure 2) records the transition to post-glacial conditions. At some localities, basal  
82 conglomerates provide evidence of subaerial exposure followed by marine  
83 transgression. The cap carbonate closely resembles basal Ediacaran carbonates  
84 elsewhere, and marks global deglaciation, eustatic sea-level rise and connection of  
85 the basin to the sea (1, 12, 14).

86 Environmental and atmospheric conditions during deposition of W2 and W3 can  
87 be further elucidated by isotopic data from carbonate-associated sulphate in  
88 lacustrine limestones (Fig. 2 and Supplementary Figure 6). These display negative to  
89 extremely negative  $\Delta^{17}\text{O}$  values with consistent linear co-variation with  $\delta^{34}\text{S}$ ,  
90 indicating mixing of pre-glacial sulphate and isotopically light sulphate formed in a  
91  $\text{CO}_2$ -enriched atmosphere (15, 16). The observed values could reflect non-unique  
92 combinations of  $p\text{CO}_2$ ,  $p\text{O}_2$ ,  $\text{O}_2$  residence time and other factors, but a box model  
93 (17) indicates  $p\text{CO}_2$  was most likely  $\sim 10$  to 100 mbar (1 mbar = 1000 ppmv).

94 These values are far too high to permit formation of low-latitude ice sheets in the  
95 Neoproterozoic, but they are consistent with a late-stage Snowball Earth. For an ice-  
96 free Neoproterozoic Earth, model studies indicate mean terrestrial temperatures in  
97 the range 30-50°C for  $p\text{CO}_2 = 10$  to 100 mbar (18). Formation of low-latitude ice  
98 sheets requires much lower  $p\text{CO}_2$ , on the order of 0.1 - 1 mbar (2, 19, 20). Once  
99 formed, however, ice sheets can persist despite rising  $\text{CO}_2$  from volcanic outgassing,  
100 due to high planetary albedo. This hysteresis in the relationship between  $p\text{CO}_2$  and  
101 planetary temperature is a key element of Snowball Earth theory. It implies that W2  
102 and W3 were deposited relatively late in the Marinoan, after volcanic outgassing had  
103 raised  $p\text{CO}_2$  from 0.1 or 1 mbar to 10 or 100 mbar. Modeled silicate weathering and  
104 volcanic outgassing rates indicate that this would require  $10^6$  to  $10^7$  years (21).

105 The consistent co-variation of  $\Delta^{17}\text{O}$  and  $\delta^{34}\text{S}$  in lacustrine limestones in both W2  
106 and W3 suggests no detectable rise in atmospheric  $p\text{CO}_2$ , as this would alter the  
107 slope of the mixing line (Fig. 2). This implies that the glacier oscillations recorded in  
108 W2 and W3 occurred during a relatively short time interval ( $<10^5$  years, 21) toward  
109 the end of the Marinoan. In turn, this implies that the remainder of the Wilsonbreen  
110 Formation (including the basal weathering horizon) represents many millions of  
111 years, during which  $p\text{CO}_2$  built up from the low values necessary for inception of low-  
112 latitude glaciation to those indicated by the geochemical evidence. The weathering  
113 horizon provides direct evidence of cold, arid conditions during this interval, prior to  
114 the appearance of fluvial and glacial lacustrine sediments in the basin.

115 The evidence for ice-sheet advance/retreat cycles at low latitudes in a  $\text{CO}_2$ -  
116 enriched atmosphere motivated a series of numerical simulations to test the  
117 hypothesis that these cycles were linked to Milankovitch orbital variations. We

118 employed asynchronous coupling of a 3D ice sheet model and an Atmospheric  
119 General Circulation Model using the continental configuration of (22). We first ran  
120 simulations with a modern orbital configuration to examine ice-sheet behaviour  
121 through a large range of  $p\text{CO}_2$  values from 0.1 to 100 mbar (23; Supplementary  
122 Figures 7-10). Consistently with previous results (2, 20), at low  $p\text{CO}_2$  (0.1 mbar),  
123 global ice volume reaches  $170 \times 10^6 \text{ km}^3$  but substantial tropical land areas remain  
124 ice free due to sublimation exceeding snowfall (Supplementary Figure S10a). Ice  
125 volume remains relatively constant for  $p\text{CO}_2 = 0.1$  to 20 mbar (Supplementary Figure  
126 S10b), due to an increase in accumulation that compensates for higher ablation rates  
127 (Supplementary Figure 13). In contrast, above 20 mbar, ice extent in the eastern  
128 Tropics significantly decreases (Supplementary Figure 10c). At  $p\text{CO}_2 = 100$  mbar,  
129 most of the continental ice cover disappears except for remnants over mountain  
130 ranges (Supplementary Figure 10d).

131 To test the sensitivity of the tropical ice sheets to Milankovitch forcing,  
132 experiments with changing orbital parameters were initialized using the steady-state  
133 ice sheets for  $p\text{CO}_2 = 20$  mbar. Although obliquity has been invoked as a possible  
134 cause of Neoproterozoic glaciations (24), this mechanism remains problematical and  
135 cannot account for significant climatic oscillations at low latitudes (25, 26). We  
136 therefore focused on precession as a possible driver, and used two opposite orbital  
137 configurations favoring cold and warm summers, respectively, over the northern  
138 tropics (CSO: cold summer orbit and WSO: warm summer orbit) (Supplementary  
139 Figure 14). Switching between these configurations causes tropical ice-sheets to  
140 advance/retreat over several hundred kilometers in 10 kyr (Supplementary Movie 1),  
141 with strong asymmetry between hemispheres (Fig. 3). Shifting from WSO to CSO

142 causes ice retreat in the southern hemisphere and ice sheet expansion in the  
143 northern hemisphere (Supplementary Figure 14c-d). Significant ice volume changes  
144 occur between 30° N and S, but are less apparent in higher latitudes. This reflects  
145 higher ablation rates in the warmer low latitudes (Supplementary Figure 14e-h), and  
146 higher ice-sheet sensitivity to shifting patterns of melt. Larger greenhouse forcing at  
147 the end of the Snowball event implies increasing ice-sheet sensitivity to subtle  
148 insolation changes. Given a strong diurnal cycle (23), our simulations also predict a  
149 significant number of days above 0°C in the tropics (Supplementary Figure 15),  
150 consistent with geological evidence for ice rafting, liquid water in lakes and rivers,  
151 and photosynthetic microbial communities.

152 Our results show that geological evidence for glacial-interglacial cycles (5-7) is  
153 consistent with an enriched Snowball Earth theory. Termination of the Marinoan  
154 panglaciation was not a simple switch from icehouse to greenhouse states but was  
155 characterized by a climate transition during which glacial cycles could be forced by  
156 Milankovitch orbital variations. The geochemical evidence presented here implies  
157 that at least the upper 60-70% of the Wilsonbreen Formation was deposited in  $\sim 10^5$   
158 years, on the assumption that a trend in  $p\text{CO}_2$  would be evident over longer  
159 timescales (21). Rates of  $\text{CO}_2$  build-up, however, may have slowed in the later stages  
160 of Snowball Earth due to silicate weathering of exposed land surfaces, so it is  
161 possible that the oscillatory phase was more prolonged.

162 Initiation of low latitude glaciation in the Neoproterozoic requires low  $p\text{CO}_2$  (0.1 -  
163 1 mbar, 2, 19, 20), implying that the oscillatory phase was preceded by a prolonged  
164 colder period ( $\sim 10^6$  to  $10^7$  years) during which  $p\text{CO}_2$  gradually increased by volcanic  
165 outgassing (21). This timescale is in agreement with recent dates indicating the

166 Marinoan lasted ~15 million years (27). The basal weathering horizon is consistent  
167 with a period of low temperatures and limited hydrological cycle prior to the  
168 oscillatory phase (2, 19).

169 Additional work is needed to refine the upper and lower limits of  $p\text{CO}_2$  conducive  
170 to climate and ice-sheet oscillations in Snowball Earth. Factors not included in the  
171 present model, such as supraglacial dust or areas of ice-free tropical ocean (28-30),  
172 can be expected to make the Earth system more sensitive to orbital forcing. While  
173 many details remain to be investigated, our overall conclusions remain robust.

174 The Neoproterozoic Snowball Earth was nuanced, varied and rich. We anticipate  
175 that detailed studies of the rock record in other parts of the world, in conjunction  
176 with numerical modeling studies, will continue to yield insight into the temporal and  
177 regional diversity of this pivotal period in Earth history.

178

179

## 180 **Methods**

181

182 **Sedimentology.** Lithofacies were classified based on grain size, internal sedimentary  
183 structures and deformation structures, and bounding surfaces. Detailed stratigraphic  
184 logs were made in the field, supplemented by drawings and photographs of key  
185 features. Samples were taken for polishing and thin sectioning, to allow detailed  
186 examination of microstructures in the laboratory. In addition, data were collected on  
187 clast lithology, shape, surface features and fabric. Diamictites of the Wilsonbreen  
188 Formation are commonly very friable, allowing included clasts to be removed intact  
189 from the surrounding matrix, allowing measurement of both clast morphology and

190 orientation, using methods developed for unlithified sediments. Clast morphology  
191 (shape, roundness and surface texture) was measured for samples of 50 clasts to  
192 determine transport pathways. Clast fabric analysis was performed by measuring a-  
193 axis orientations of samples of 50 clasts with a compass-clinometer, and data were  
194 summarized using the eigenvalue or orientation tensor method. Orientated samples  
195 for measurement of Anisotropy of Magnetic Susceptibility (AMS) were collected  
196 using a combination of field-drilling and block sampling. AMS was measured using an  
197 AGICO KLY-3 Kappabridge operating at 875 Hz with a 300 A/m applied field at the  
198 University of Birmingham and an AGICO MFK-1A Kappabridge operating at 976 Hz  
199 with a 200 A/m applied field at New Mexico Highlands University.

200

201 **Geochemistry.** Laboratory procedures for extracting, purifying, and measuring the  
202 triple oxygen ( $\delta^{18}\text{O}$  and  $\Delta^{17}\text{O}$ ) and sulfur ( $\delta^{34}\text{S}$ ) isotope composition of CAS in bulk  
203 carbonates are detailed in ref 16. Briefly, fresh carbonate-bearing rock chips were  
204 crushed into fine grains and powders using mortar and pestle. Rinsing the fines with  
205 18 M $\Omega$  water revealed little water-leachable sulphate in all the Wilsonbreen  
206 carbonates. Subsequently, ca. 10 to 30 g carbonates were slowly digested in 1-3 M  
207 HCl solutions. The solution was then centrifuged, filtered through a 0.2  $\mu\text{m}$  filter, and  
208 acidified before saturated  $\text{BaCl}_2$  droplets were added.  $\text{BaSO}_4$  precipitates were  
209 collected after >12 hours and purified using the DDARP method (see Supporting  
210 Information). The purified  $\text{BaSO}_4$  was then analyzed for three different isotope  
211 parameters: 1)  $\Delta^{17}\text{O}$ , by converting to  $\text{O}_2$  using a  $\text{CO}_2$ -laser fluorination method; 2)  
212  $\delta^{18}\text{O}$ , by converting to CO through a Thermal Conversion Elemental Analyzer (TCEA)  
213 at 1450  $^\circ\text{C}$ ; and 3)  $\delta^{34}\text{S}$ , by converting to  $\text{SO}_2$  by combustion in tin capsules in the

214 presence of V<sub>2</sub>O<sub>5</sub> through an Elementar Pyrocube elemental analyzer at 1050 °C. The  
215  $\Delta^{17}\text{O}$  was run in dual-inlet mode while the  $\delta^{18}\text{O}$  and  $\delta^{34}\text{S}$  in continuous-flow mode.  
216 Both the  $\Delta^{17}\text{O}$  and  $\delta^{18}\text{O}$  were run on a MAT 253 at Louisiana State University whilst  
217 the  $\delta^{34}\text{S}$  was determined on an Isoprime 100 continuous flow mass spectrometer at  
218 the University of Lancaster, UK. The  $\Delta^{17}\text{O}$  was calculated as  $\Delta^{17}\text{O} \equiv \delta'^{17}\text{O} - 0.52 \times \delta'^{18}\text{O}$   
219 in which  $\delta' \equiv 1000 \ln (R_{\text{sample}}/R_{\text{standard}})$  and R is the molar ratio of  $^{18}\text{O}/^{16}\text{O}$  or  $^{34}\text{S}/^{32}\text{S}$ .  
220 All  $\delta$  values are in VSMOW and VCDT for sulphate oxygen and sulfur respectively.  
221 The analytical standard deviation ( $1\sigma$ ) for replicate analysis associated with the  $\Delta^{17}\text{O}$ ,  
222  $\delta^{18}\text{O}$ , and  $\delta^{34}\text{S}$  are  $\pm 0.05\text{‰}$ ,  $\pm 0.5\text{‰}$ , and  $\pm 0.2\text{‰}$ , respectively. Since the CAS is  
223 heterogeneous in hand-specimen, the standard deviation is for laboratory  
224 procedures.  $\delta^{34}\text{S}$  values were corrected against VCDT using within run analyses of  
225 international standard NBS-127 (assuming  $\delta^{34}\text{S}$  values of +21.1 ‰). Within-run  
226 standard replication (1 SD) was  $< 0.3 \text{‰}$ . All geochemical data are included in  
227 Supplementary Table 1.

228

229 **Numerical modeling.** Model runs were conducted with a coupled atmospheric  
230 general circulation model (LMDz) and ice-sheet model (GRISLI: GRenoble Ice Shelf  
231 and Land Ice model). LMDz (spatial resolution 4° in latitude x 5° in longitude with 38  
232 vertical levels) was run with prescribed continental ice to climatic equilibrium. GRISLI  
233 has a 40km grid size and is driven with downscaled climatic fields of surface air  
234 temperature, precipitation and evaporation. To capture ice sheet – climate  
235 feedbacks, LMDz is rerun using the new ice sheet distribution and topography. This  
236 procedure was repeated each 10 kyr to investigate orbital forcing.

237

238 Surface mass balance (accumulation minus sublimation and melting) was computed  
239 from monthly mean temperature, precipitation and evaporation rate. Melt rate is  
240 calculated using the Positive Degree Day method.

241

242 No sea ice dynamics treatment is specified, the sea ice cover is prescribed and a  
243 thickness of 10 meters is imposed. Ice albedo is fixed at 0.6, while snow albedo  
244 varies from 0.9 from 0.55 as a function of the zenith, and ageing process. Land  
245 ice/snow free surface has the characteristic of a bare soil (rocky regolith) with an  
246 albedo of 0.3.

247

248 Code availability. Code for the GCM LMDz can be accessed at:  
249 <http://lmdz.lmd.jussieu.fr>. Code for the ISM GRISLI (GRenoble Ice Shelf and Land Ice  
250 model) is not available.

251

252 Additional details of the methods and modeling procedures are provided in the  
253 Supplementary Information in the online version of the paper.

254

255

## References

- (1) Hoffman, P.F. and Schrag, D.P. The Snowball Earth hypothesis: testing the limits of global change. *Terra Nova* **14**, 129-155 (2002).
- (2) Donnadieu, Y., Godd ris, Y. and Le Hir, G. Neoproterozoic atmospheres and glaciation. In: *Treatise on Geochemistry*, Second Edition Vol. 6, 217-229 (2014).
- (3) Hoffman, P.F. Strange bedfellows: glacial diamictite and cap carbonate from the Marinoan (635Ma) glaciation in Namibia. *Sedimentology* **58**, 57-119 (2011).
- (4) Allen, P.A. and Etienne, J.L. Sedimentary challenge to Snowball Earth. *Nat Geosci* **1**, 817-825 (2008).
- (5) Rieu, R., Allen, P.A., Pl tze, M. and Pettke, T. Climatic cycles during a Neoproterozoic "snowball" glacial epoch. *Geology* **35**, 299-302 (2007).
- (6) Le Heron, D.P., Busfield, M.E., and Kamona, F. An interglacial on snowball Earth? Dynamic ice behaviour revealed in the Chuos Formation, Namibia. *Sedimentology* **60**, 411-427 (2013).
- (7) Fairchild, I.J. and Hambrey, M.J. Vendian basin evolution in East Greenland and NE Svalbard. *Precambrian Res* **73**, 217-233 (1995).
- (8) Halverson, G.P. A Neoproterozoic Chronology IN: Xiao, S. & Kaufman, A.J. (Eds.) *Neoproterozoic Geobiology and Paleobiology*, 231-271 (Springer, New York, 2006).
- (9) Li, X.-X., Evans, D.A. and Halverson, G.P. Neoproterozoic glaciations in a revised global palaeogeography from the breakup of Rodinia to the assembly of Gondwanaland. *Sediment Geol* **294**, 219-232 (2013).

(10) Petronis, M S, Stevenson, C, Fleming, E J, Fairchild, I J, Hambrey, M, Benn, D I., 2013, Paleomagnetic Data from the Neoproterozoic Wilsonbreen Formation, Ny Friesland, Svalbard, Norway and Preliminary Data from the Storeelv Formation, Ella Ø, Kong Oscar Fjord, East Greenland, American Geophysical Union, Fall Meeting 2013, abstract #GP41A-1107.

(11) Harland, W.B. *The Geology of Svalbard*. Geol. Soc. London Mem., 17 (Geological Society, London, 1997).

(12) Creveling, J.R. and Mitrovica, J.X. The sea-level fingerprint of a Snowball Earth deglaciation. *Earth Planet Sc Lett* **399**, 74–85 (2014).

(13) Lyons, W.B. et al. The McMurdo Dry Valleys long-term ecological research program: new understanding of the biogeochemistry of the Dry Valley lakes: a review. *Polar Geography* **25**, 202-217 (2001).

(14) Hoffman, P. et al. Are basal Ediacaran (635 Ma) basal 'cap dolostones' diachronous? *Earth Planet Sc Lett* **258**, 114-131 (2007).

(15) Fairchild, I.J., Hambrey, M.J., Spiro, B. and Jefferson, T.H. Late Proterozoic glacial carbonates in northeast Spitsbergen: new insights into the carbonate-tillite association. *Geol Mag* **126**, 469-490 (1989).

(16) Bao, H., Fairchild, I.J, Wynn, P.M. and Spötl, C. Stretching the envelope of past surface environments: Neoproterozoic glacial lakes from Svalbard. *Science* **323**,119-122 (2009).

(17) Cao, X. and Bao, H. Dynamic model constraints on oxygen-17 depletion in atmospheric O<sub>2</sub> after a Snowball Earth. *P Natl Acad Sci USA* **110**, 14546–14550 (2013).

(18) Le Hir, G. et al. The snowball Earth aftermath: Exploring the limits of continental weathering processes. *Earth Planet Sc Lett* **277**, 453–463 (2009).

(19) Pierrehumbert, R., Abbot, D.S., Voigt, A. and Koll, D. Climate of the Neoproterozoic. *Ann Rev Earth Planet Sci* **39**, 417-460 (2011).

(20) Pollard, D. and Kasting, J.F. Climate-ice simulations of Neoproterozoic glaciation before and after collapse to Snowball Earth. In: G.S. Jenkins, M.A.S. McMenamin, C.P. McKay and L. Sohl (eds.) *The Extreme Proterozoic: Geology, Geochemistry, and Climate*. Geophys. Monogr. Ser. 146 (AGU, Washington, D.C. 2004).

(21) Le Hir, G., Ramstein, G., Donnadiieu, Y. and Godd ris, Y. Scenario for the evolution of atmospheric pCO<sub>2</sub> during a snowball Earth. *Geology* **36**, 47–50 (2008).

(22) Hoffman, P.F., Li, Z.X., A palaeogeographic context for Neoproterozoic glaciation. *Palaeogeogr Palaeocl* **277**, 158–172 (2009).

(23) Pierrehumbert, R.T. Climate dynamics of a hard Snowball Earth. *J Geophys Res* **110**, DOI: 10.1029/2004JD005162 (2005).

(24) Spiegl, T. C., Paeth, H. and Frimmel, H.E., Evaluating key parameters for the initiation of a Neoproterozoic Snowball Earth with a single Earth System Model of intermediate complexity. *Earth Planet Sc Lett* **415**, 100-110 (2015).

(25) Donnadiieu, Y., Ramstein, G., Fluteau, F., Besse, J. and Meert, J. Is high obliquity a plausible cause for Neoproterozoic glaciations? *Geophys Res Lett* **29**, DOI: 10.1029/2002GL015902 (2002).

(26) Paillard, D. Quaternary glaciations: from observations to theories. *Quaternary Sci Rev* **107**, 11-24 (2015).

(27) Rooney, A.D. et al. A Cryogenian chronology: Two long-lasting synchronous Neoproterozoic glaciations. *Geology* 43, 459-462 (2015).

(28) Abbot, D.S. and Pierrehumbert, R.T. Mudball: surface dust and Snowball Earth deglaciation. *J Geophys Res* **115**, DOI: 10.1029/2009JD012007 (2010).

(29) Abbot, D.S., Voigt, S. and Koll, D. The Jormungand global climate state and implications for Neoproterozoic glaciations. *J Geophys Res-Atmos* 116, DOI: 10.1029/2011JD015927 (2011).

(30) Rose, B. E. J. Stable “Waterbelt” climates controlled by tropical ocean heat transport: A nonlinear coupled climate mechanism of relevance to Snowball Earth. *J Geophys Res-Atmos* **120**, doi:10.1002/2014JD022659 (2015).

Correspondence and requests for materials should be addressed to Doug Benn (doug.benn@unis.no).

### **Acknowledgements**

This work was supported by the NERC-funded project GR3/ NE/H004963/1 Glacial Activity in Neoproterozoic Svalbard (GAINS). Logistical support was provided by the University Centre in Svalbard. This work was granted access to the HPC resources of CCRT under allocation 2014-017013 made by GENCI (Grand Equipement National de Calcul Intensif). We also thank Didier Paillard and Paul Hoffman for stimulating discussions and valuable insights.

### **Author contributions**

Field data were collected and analyzed by IJF, DIB, EJF, MJH, EAMcM, MSP, PMW and CTES. Geochemical analyses were conducted by HB and PMW. Model experiments were designed and conducted by GLeH, YD, CD and GR. The manuscript and figures were drafted by DIB, IJF and GLeH, with contributions from the other authors.

### **Competing financial interests**

The authors declare no competing financial interests.

## Figures:

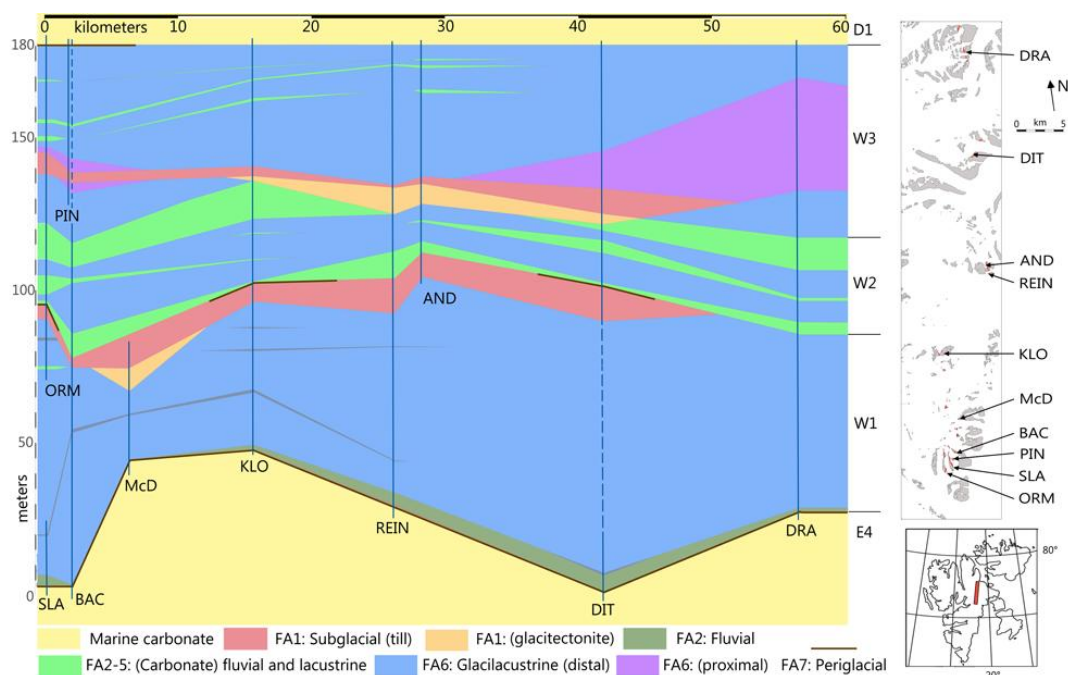


**Figure 1: Sedimentary architecture and palaeoenvironments of the Wilsonbreen**

**Formation.** Regional correlation of facies associations and members W1, W2 and W3

across NE Svalbard. From north to south, study locations are: DRA: Dracoisen; DIT:

Ditlovtoppen; AND: East Andromedafjellet; REIN: Reinsryggen (informal name); KLO:

Klofjellet; McD: MacDonaldryggen; BAC: Backlundtoppen - Kvitfjellet ridge; PIN:

Pinnsvinryggen (informal name); SLA: Slangen and ORM: Ormen.

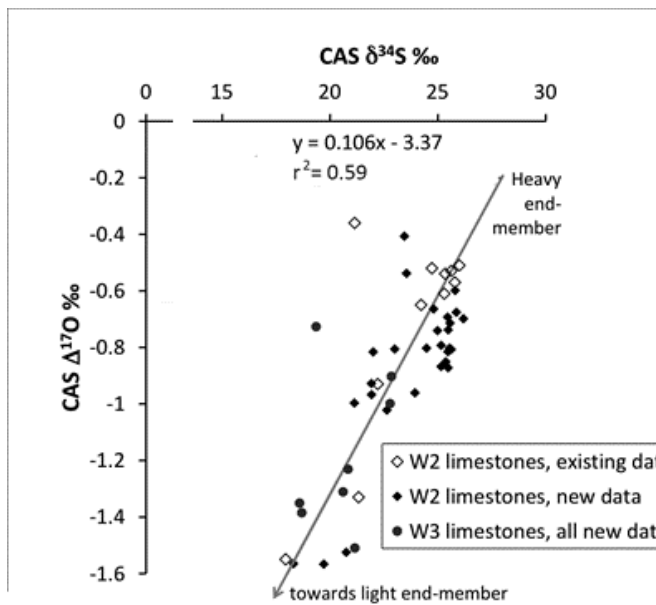


**Figure 2: Co-variation of  $\Delta^{17}\text{O}$  and  $\delta^{34}\text{S}$  from carbonate-associated sulphate in W2 and W3.** Existing data (ref. 16) and new data define a mixing line between pre-glacial sulphate (top) and an isotopically light sulphate formed by oxidation of pyrite including incorporation of a light- $\Delta^{17}\text{O}$  signature from a  $\text{CO}_2$ -enriched atmosphere. Data from W2 and W3 lie on closely similar trend lines, indicating no detectable change in  $\text{pCO}_2$  between deposition of the two members.

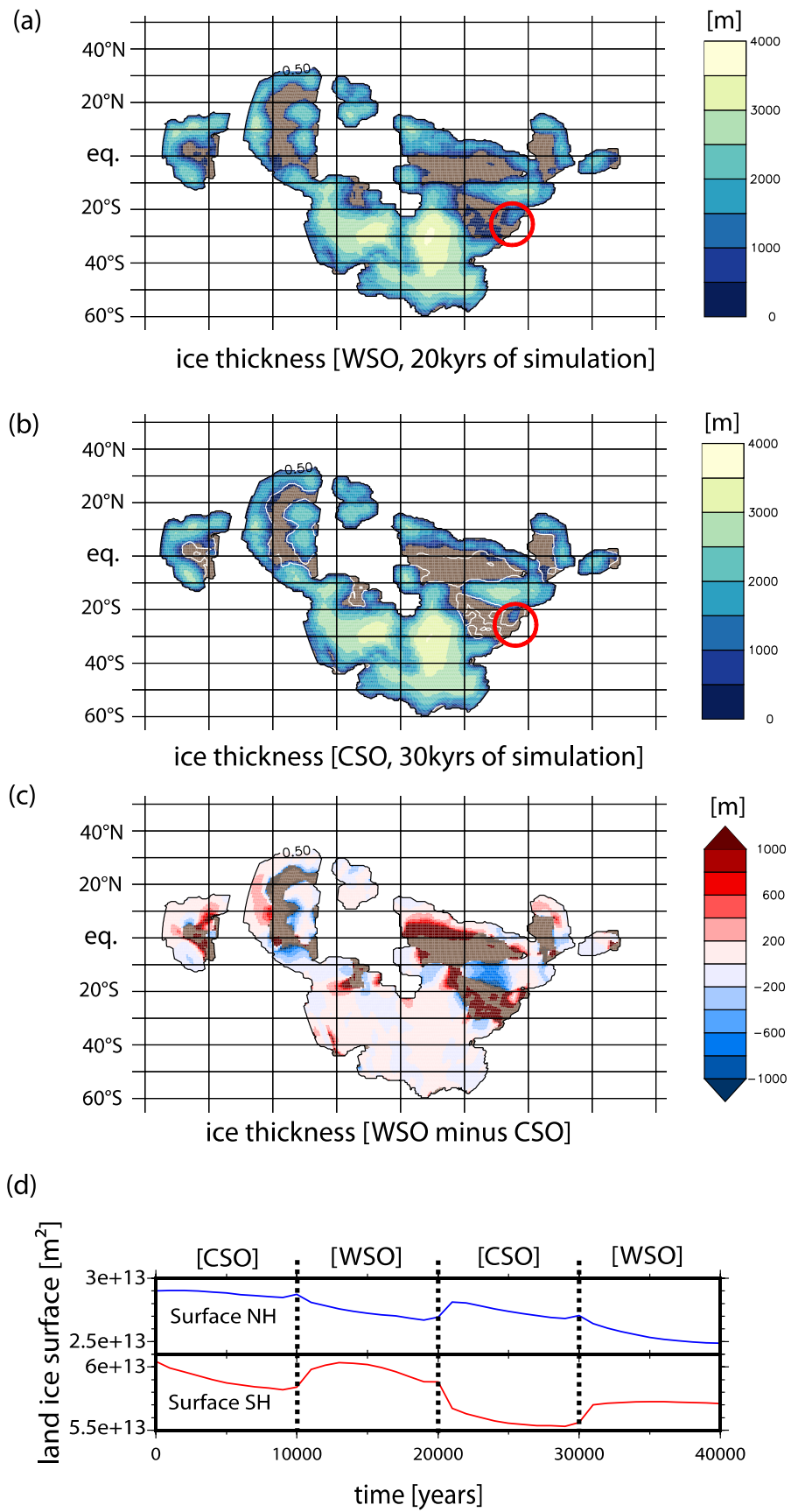


**Figure 3: Modelled ice sheet oscillations in response to orbital forcing. (a), (b) Land**

ice thickness obtained with 20 mbar of carbon dioxide in response to changes of orbital forcing (WSO and CSO, warm/cold summer orbit for the northern hemisphere) over the course of two precession cycles (40 ky of simulation).

Continental areas without ice are light brown, the white line is used to represent the old ice-sheet extension (WSO case). The Svalbard area is indicated by a red circle. (c)

ice thickness variation in 10 ky (WSO case after 20 ky minus CSO case after 30 ky of simulation) (d) area covered by ice ( $m^2$ ) in each hemisphere through time ([WSO] and [CSO] indicate which orbital configuration is used).